Longitudinal variation in Global Navigation Satellite Systems TEC and topside ion density over South American sector associated with the four-peaked wave structures

P. A. B. Nogueira,[1] M. A. Abdu,[1] J. R. Souza,[1] G. J. Bailey,[2] I. S. Batista,[1] E. B. Shume,[3] and C.M. Denardini [1]

Received 31 July 2013; revised 25 November 2013; accepted 2 December 2013; published 27 December 2013.

[1] Recent observations of the low-latitude ionospheric electron density revealed a four-peaked longitudinal structure in the equatorial ionization anomaly when plotted at a constant-local-time frame. It was proposed that neutral wind-driven *E* region dynamo electric fields due to nonmigrating tidal modes are responsible for this pattern. We examine the four-peaked structure in the observed topside ion density and its manifestation as longitudinal structures in total electron content (TEC) over South America. The strong longitudinal variation in TEC characterized by larger value over Brazilian eastern longitude sector as compared to that over the Peruvian western longitude is modeled using the Sheffield University plasmasphere-ionosphere model (SUPIM) aiming to identify the control factors responsible for the longitude variation. We found that the SUPIM runs using as input the existing standard models of vertical drift, and thermospheric winds do not explain the TEC longitudinal structure. Realistic values of these control parameters were generated based on the strong vertical drift longitudinal variation as determined from magnetometer and Digisonde data and appropriately adjusted winds (horizontal wind model). These realistic vertical drifts together with the modified thermospheric wind, when used as input to the SUPIM, are found to satisfactorily explain the longitudinal differences in the TEC and topside ion density (Ni) over South America. The study shows that the TEC in the whole latitude distribution is larger over the east coast than over the west coast of South America and that the vertical drift and thermospheirc winds control the longitudinal four wave structure in the TEC and Ni.

Citation: Nogueira, P. A. B., M. A. Abdu, J. R. Souza, G. J. Bailey, I. S. Batista, E. B. Shume, and C. M. Denardini (2013), Longitudinal variation in Global Navigation Satellite Systems TEC and topside ion density over South American sector associated with the four-peaked wave structures, *J. Geophys. Res. Space Physics*, *118*, 7940–7953, doi:10.1002/2013JA019266.

1. Introduction

[2] Recent observation and modeling studies of the low-latitude ionosphere have revealed a four-peaked longitudinal structure in its key parameters: the electron density, electric field, and thermospheric neutral wind [*England et al*., 2006; *Immel et al*., 2006; *Kil et al*., 2008; *Lin et al*., 2007a, 2007b; *Bankov et al*., 2009; *Liu and Watanabe*, 2008; *Lühr et al*., 2007, 2008; *Scherliess et al*., 2008; *Wan et al*., 2008; *Pedatella et al*., 2011; *Oberheide et al*., 2011; *Hagan et al*., 2007; *Häusler et al*., 2010; *Hartman and Heelis*, 2007]. *Sagawa et al*. [2005] were the first to suggest a relation between longitudinal variation in the electron density and vertical propagation of nonmigrating tides. Through comparison with the seasonal variation of the different nonmigrating tidal modes, the wave number 4 signature in the ionosphere has been attributed to the eastward propagating diurnal nonmigrating tide with zonal wave number 3 (DE3) [e.g., *Forbes et al*., 2008; *Pancheva and Mukhtarov*, 2010]. According to *Immel et al*. [2006], the mechanism by which the DE3 tide may introduce a longitudinal variability into the low-latitude ionosphere is by the modulation of the daytime ionospheric wind dynamo, which generates the low-latitude electric fields and currents in the *E* region ionospheric dynamo. It results in a longitudinal modulation of the low-latitude electric field that drives the equatorial ionization anomaly (EIA). The corresponding longitudinal modulation in the EIA strength is characterized by enhanced EIA crest densities with larger latitudinal separation of the crests occurring in specific longitude sectors along the low-latitude region [e.g., *Immel et al*., 2006]. The DE3 tide has also been shown to be penetrating directly to thermospheric and exospheric height [*Forbes et al*., 2009; *Oberheide et al*., 2011] thereby playing a critical role in causing longitudinal variation in the topside ionospheric total electron content (TEC).

[1]Divisão de Aeronomia, Instituto Nacional de Pesquisas Espaciais, São José dos Campos, Brazil.
[2]Department of Applied Mathematics, The University of Sheffield, Sheffield, UK.
[3]Jet Propulsion Laboratory, California Institute of Technology, Pasadena, California, USA.

Corresponding author: P. A. B. Nogueira, Divisão de Aeronomia/Instituto Nacional de Pesquisas Espaciais, Av. dos Astronautas, 1758, Jd. da Granja, 12227–010 São José dos Campos, São Paulo, Brazil. (paulo@dae.inpe.br)

2169-9380/13/10.1002/2013JA019266

Table 1. Ground Station Locations

Station	Latitude	Longitude	Dip Angle
Arequipa	−16.4°	288.5°	−7°
São Luís	−2.5°	315°	−1.3°
Jicamarca	−11.95°	283.13°	1.16°
Salta	−24.78°	294.6°	−24°
São José dos Campos	−23.17°	314.11°	−32°
Piura	−5.169°	279.36°	13.56°
Eusébio	−3.89°	321.56°	10.6°

[3] *Oberheide et al*. [2011] have discussed that the four-peaked structure in the TEC may not be attributed entirely to the DE3 nonmigrating tides. The effects of wave contributions may arise also from the nonmigrating tidal modes: DW5, SW6, SE2, TW7, and TE1, as well as from the stationary planetary wave number 4, where the first letter describe the period, i.e., D for Diurnal, S for semidiurnal, and T stands for terdiurnal tides; the second letter represent the westward (W) or eastward (E) propagating diurnal tide; and the number is indicating the wave number. *Lühr et al*. [2008] and *England et al*. [2006] have presented and discussed results only for the months of September and October, which happen to be dominated by the DE3 nonmigrating tidal amplitude [see also *Pedatella et al*., 2011].

[4] The main aims of the present work are to analyze observational data and to understand the formation of the four-peaked structure in the equatorial and low-latitude ionosphere, especially focusing on the longitudinal variation of the TEC in the South American longitude sector, by performing model simulation studies including the effect of longitudinal modulations by the wind dynamo electric field, thermospheric neutral wind, and the ion production and loss process. The analysis was performed using observational data on the TEC as obtained from Global Navigation Satellite System (GNSS) receivers and the topside ion density as measured by the Defense Meteorological Satellite Program (DMSP) satellites. The Sheffield University plasmasphere-ionosphere model (SUPIM) was used to model the low-latitude ionosphere, for which the vertical $\mathbf{E} \times \mathbf{B}$ plasma drift, which is a key input parameter, was obtained from magnetometer and ionosonde data and from the empirical vertical drift model by *Scherliess and Fejer* [1999]. For a detailed description of the SUPIM see *Bailey et al*. [1993] and *Bailey and Balan* [1996]. The thermospheric neutral wind model, which is another key input parameter, used in the SUPIM was the horizontal wind model (HWM)-07 code [*Drob et al*., 2008]. We will show that the four-peaked structure in the equatorial ionosphere may be explained by a theoretical model that uses a realistic combination of the zonal electric field and thermospheric wind. We will further show that the significant longitudinal variation on the GNSS TEC observed in the South American longitude sector is an integral part of the four-peaked structure. In the following, we present, in section 2, descriptions of the topside Ni and the TEC data, the methods of analysis including the deduction of the daytime vertical drift from magnetometer data, and the ionospheric simulation procedure using the SUPIM. Section 3 deals with the results of analysis of the observational data and of the SUPIM simulation runs, and discussion of the results, and section 4 presents a summary and the conclusions.

2. The Database

2.1. Ion Density Data From DMSP

[5] The Defense Meteorological Satellite Program (DMSP) has provided data since the launch of the first DMSP spacecraft in January 1965. The scientific data on the Earth's ionosphere and atmosphere were obtained from particle and field detectors onboard the spacecraft. The satellites are in near-polar and circular orbits at an altitude between 835 and 850 km. The orbital inclination of the spacecraft is 96°, which results in a precession rate of one rotation per year. It results in keeping the spacecraft orbit roughly fixed in a local time throughout the year.

[6] The DMSP F13 satellite is in a roughly dawn-dusk orientation while the F12, F14, and F15 are all in a 0930–2130 local time orientation. The data from the F13 satellite in the dawn-dusk orientation is used in the present study, and the plasma density (Ni) used here was recorded at 4 s resolution.

2.2. TEC Data From GNSS

[7] The TEC data, used in this analysis, were collected by the GNSS ROGUE SNR-8000 receiver at Arequipa (AREQ), which is one of the stations of the International GNSS Service [*Dow et al*., 2005]. The receiver at AREQ located near the dip equator, on the west coast of South America, provides the TEC data based on carrier phase and pseudorange measurements at two frequencies. The data from São Luís were obtained by a GPS Turbo Rogue ICS-4000z receiver that can provide the carrier phase and two-frequency group delay TEC values. This station is located close to the dip equator on the eastern sector of South America. The geographic coordinates and the dip angle of all stations used in this study are given in Table 1. An additional concern for the calculation of the TEC values is the satellite elevation angle, as a smaller elevation angle implies a longer integration path for the total electron content and sampling at different latitude. To reduce uncertainty in the TEC values, only satellite data with elevation angle higher than 30° were selected. A detailed description of the TEC calculation can be found in *Mannucci et al*. [1998].

2.3. The E × B Vertical Drift From Magnetometers and Digisondes

[8] The daytime vertical plasma drift over the magnetic equator was calculated using the methodology described by *Anderson et al*. [2002] who derived a quantitative relationship between the daytime vertical $\mathbf{E} \times \mathbf{B}$ plasma drift and the magnetic field variation ΔH due the equatorial electrojet, where ΔH is the difference between the horizontal magnetic field component variation at a dip equatorial station and that of an off-equatorial station (within 5–6° from the dip equator). The magnetometer data used in this calculation were obtained from the magnetometers operated in São Luís (2.3°S, 44.2°W, dip angle: −1.34°) and Eusébio (3.891°S, 38.441°W, dip angle: −10.6°), for the Brazilian sector, and those of Jicamarca (11.95°S, 76.87°W, dip angle: 1.16°) and Piura (5.169°S, 80.639°W, dip angle: 13.56°) for the Peruvian sector. Such methodology has been validated for longitudinal sectors other than that of Jicamarca by *Anderson et al*. [2006]. *Denardini et al*. [2011] have used the $\mathbf{E} \times \mathbf{B}$ drift calculation from magnetometer data for Brazilian longitudes.

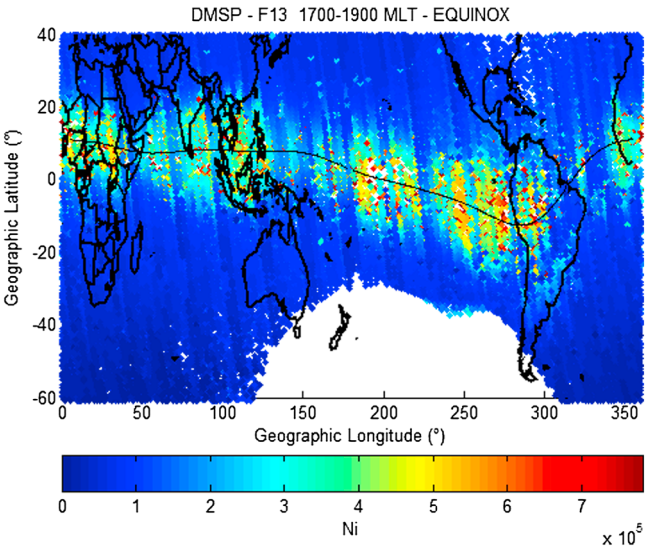

Figure 1. Geographic latitude versus longitude distribution near sunset terminator of the ion density at 840 km as measured by the DMSP-13 satellite at high solar activity epoch (2001) during the equinox. The black curve running across the plot indicates the magnetic equator.

[9] The $\mathbf{E} \times \mathbf{B}$ drift velocity derived from ΔH measurements is valid only during the daytime (from 0630 LT up to 1730 LT). For the evening hours we have used Digisonde data to calculate it from the F_2 layer peak height (hmF_2), as $Vz = \frac{\mathrm{d}(\mathrm{hm}F2)}{\mathrm{d}t}$. This methodology has been shown to be valid near sunset and nighttime hours when the F layer height is above a threshold of 300 km. At lower altitudes the effect of the recombination can make the calculated drift an apparent vertical drift [*Bittencourt and Abdu*, 1981]. However, at the high solar activity period (2001) of the present study, the F layer peak height is usually higher than 300 km during the evening and post sunset hours. For the $\mathbf{E} \times \mathbf{B}$ drift velocity between 2200 LT and 0630 LT we assumed that the ratio of the vertical drifts between Jicamarca and São Luís is maintained during the daytime and nighttime, which means that in the case that the daytime vertical drift over Jicamarca is, for example, approximately twice that over São Luís, the nighttime vertical drift at Jicamarca was also considered twice the vertical drift over São Luís. Actually, we used, as a reference, the *Scherliess and Fejer* [1999] electric field model that was then modified according to the above criteria. To avoid discontinuity in the daily $\mathbf{E} \times \mathbf{B}$ variation we have smoothed the values at the transition regions of the three different methods.

[10] For the case of Jicamarca/Arequipa the daytime vertical drift inferred from the Jicamarca-Piura magnetometer data and the evening vertical drift obtained from hmF_2 data are quite similar to the drift values obtained from *Scherliess and Fejer* [1999] empirical model. Thus, the overall vertical drift model we have used can be considered to be a reliable representation of the true vertical plasma drifts for the Peruvian as well as for the Brazilian longitude sectors.

2.4. Model Simulations by the SUPIM

[11] The SUPIM is a theoretical first principle model that can provide reliable representations of the density and temperature distributions of the important ion species in the ionosphere and plasmasphere [*Bailey et al*., 1978, 1993; *Bailey and Sellek*, 1990; *Bailey and Balan*, 1996]. It is a two-dimensional model that solves the time-dependent equations of continuity, momentum, and energy balance along closed magnetic field lines to obtain values of the densities, field-aligned velocities, and temperatures of the ions and electrons. The magnetic field model used in the SUPIM is an eccentric dipole representation. The offset between the magnetic and geographic poles and the magnetic declination angle were introduced using the spherical harmonic expansion of the geomagnetic scalar potential as per the International Geomagnetic Reference Field (IGRF). The main physical, photochemical, and dynamical processes include the following: ion production due to the solar EUV radiation, ion production and loss due to chemical reactions, ambipolar and thermal diffusion, ion-ion and ion-neutral collisions, thermospheric neutral winds, plasma drift, thermal conduction, photoelectron heating, frictional heating, and a number of local heating and cooling mechanisms (for more details see *Bailey et al*. [1997] and *Bailey and Balan* [1996]). See also *Souza et al*. [2000a] for applications of the model to low latitudes over Brazil. The SUPIM uses the neutral temperature and gas concentrations taken from the NRLMSIS-00 atmosphere model [*Picone et al*., 2002]. The solar EUV fluxes input in the model was adopted from the EUVAC solar EUV flux model for aeronomic calculations (EUVAC) model of *Richards et al*. [1994]. The zonal component of the $\mathbf{E} \times \mathbf{B}$ drift was neglected as it has negligible effects on electron density profiles [*Balan et al*., 1996].

3. Results and Discussion

[12] Figure 1 presents a latitude versus longitude plot of the ion density distribution at 840 km as observed by the DMSP-F13 satellite (the data were obtained from the DMSP Special Sensor for Ions, Electrons, and Scintillation (SSIES) Data Distribution at UT-Dallas) at 1745 LT time frame (LT stands for local time), for the period September to October 2001. The color coding depicts the ion density, while the black curve denotes the position of the magnetic equator.

[13] The ion density distribution in Figure 1 presents a strong longitudinal variation, highlighting the well-known four-peaked structure in the equatorial ionosphere. It can be noted that the regions of enhanced Ni values occur close to the following longitudinal sectors: 350°–30° (West Africa), 90°–120° (India and Southeast Asia), 180°–200° (Central Pacific), and 240°–290° (west of South America). It may be noted that these longitudinal positions of the Ni maxima agree well with those of the ionospheric TEC as observed by the COSMIC satellites during September equinox when the F region ionosphere is known to exhibit a primarily wave number 4 structure attributed to forcing by DE3 tide [*Pedatella et al*., 2011]. A strong longitudinal variation of the ion density over the South America, which is a part of this four wave structure, is noteworthy. This region is also well known as being characterized by a strong longitudinal variation in the magnetic declination and by the presence of the South Atlantic/American Magnetic Anomaly [*Abdu et al*., 2005]. Such variation in the magnetic field strength and declination angle may reflect in the magnitudes of vertical $\mathbf{E} \times \mathbf{B}$ drift and the thermospheric winds that may cause season-dependent modification in the plasma density distribution and TEC in the topside ionosphere as shown by *Pedatella et al*. [2011].

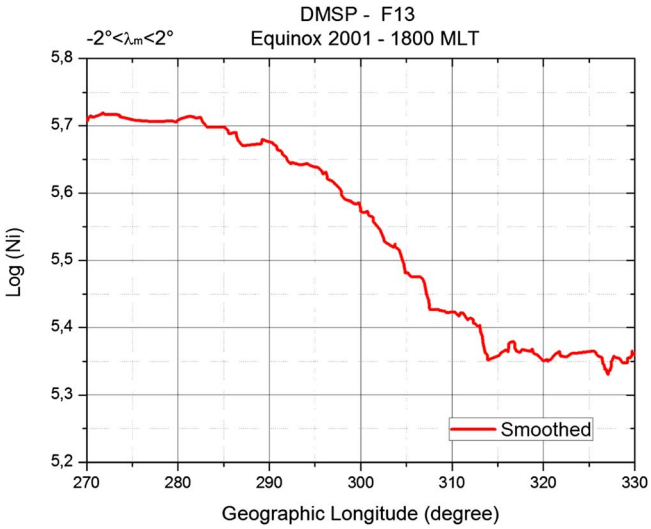

Figure 2. The ion density variation at 840 km over the magnetic equator in the longitude region of South America as obtained from the DMSP-F13.

[14] Aiming to understand the detailed nature of this strong longitudinal variation in the ion density, a meridional averaging of the Ni values within a small-latitude range $-2° < \lambda_{mag} < 2°$ (where λ_{mag} means magnetic latitude) was performed; a running average was taken to smooth the data within this latitude range. The logarithm of the smoothed ion density was plotted as a function of the longitude from 270°E up to 330°E (South America) in Figure 2. This figure shows a longitudinal cut of the evening sector equatorial topside ion density over South America as sampled by the DMSP-13 satellite. Figure 2 clearly demonstrates that the ion density in the topside ionosphere (840 km) substantially decreases from the west coast toward the east coast of South America. In absolute terms, the Ni values over west coast are a factor of about 2.5 higher than the values over the east coast.

[15] In order to better understand the nature of this strong longitudinal variation in the Ni values over South American sector, we have undertaken an analysis of the GNSS TEC variations at two stations located close to the extremities of the considered longitude range and near the magnetic equator in Peru and Brazil. These stations are Arequipa, Peru (−16.40°; 288.5°; *dip angle*: −7° (2001)), and São Luís, Brazil (−2.5°; 315°, *dip angle*: −1.3° (2001)), shown in Figure 3, wherein the black line represents the magnetic equator as per the IGRF 11 model. It may be pointed out that the magnetic declination angle is almost nil over Arequipa as compared to its large negative value (being −19°) over São Luís. See also Table 1 showing the location of all ground station used in the present work.

[16] Our approach to understand the longitudinal variations in ion density as well as that in the TEC between Arequipa and São Luís involves comparison of the observational data with theoretical model results for the two locations.

[17] The TEC data were selected to correspond to three different solar activity levels: high solar activity represented by 2001, moderate solar activity represented by 2005, and low solar activity represented by 2007; however, only data for 2001 was subjected to detailed analysis based on the availability of data from the observational network (GNSS TEC, magnetometer, DMSP, and ionosondes). The two stations under comparison are separated by ~39° of longitude. Figure 4 shows the diurnal (24 h) variations of the observational TEC values plotted for all the days of the year 2001, where the plot in Figure 4a is for Arequipa and in Figure 4b is for São Luís. Figures 4c and 4d show the corresponding SUPIM model results (to be discussed later). It is important to mention that the TEC values were smoothed by a 9 day running average in order to eliminate the short-term and day-to-day variability, which is not the objective of the present work.

[18] The general pattern of the observational TEC diurnal variation over Arequipa and São Luís is characterized by its sharp increase after 0500 LT to reach peak values around 1400 LT followed by a slow decrease toward sunset, remaining at low values during the night. The larger TEC values during the daytime are mainly due to ionization production by the solar EUV and the upward plasma transport (by $\mathbf{E} \times \mathbf{B}$ drift) to higher altitudes of lower recombination rate. On the other hand, the lowest TEC values occur at nighttime due to the absence the EUV and the downward $\mathbf{E} \times \mathbf{B}$ drift that moves the *F* layer plasma to lower altitudes of higher recombination rate. Seasonally, the highest TEC values occur as two maxima during equinoctial months, a broad maximum around the October equinox and a narrower peak centered around March equinox. The seasonal minimum values occur in July (southern winter) solstice. A notable feature at both stations is an equinoctial asymmetry in the TEC values, the maximum of the October equinox being larger than that of the March equinox, which is noticeable more markedly over São Luís. However, the TEC values for 2005 and 2007 (not shown here) presented larger values during the March equinox for both the stations.

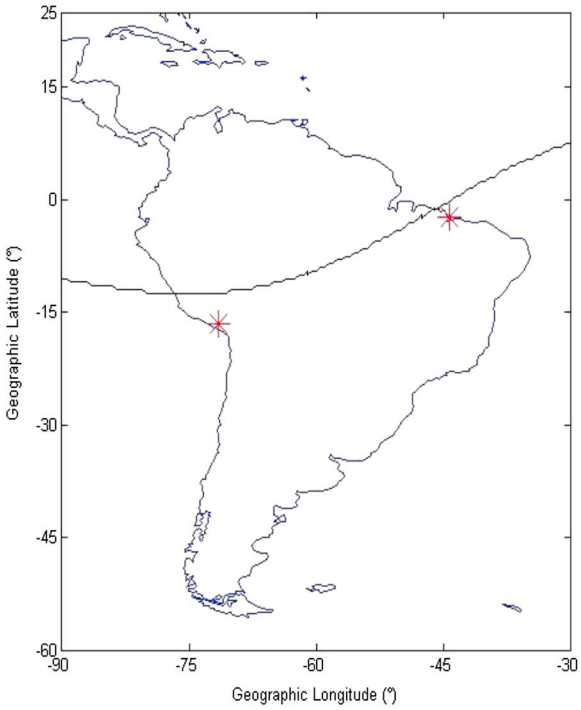

Figure 3. Locations of the dual-frequency GPS receivers (red stars) at Arequipa in the west coast of South America and at Sao Luis in Brazilian eastern sector.

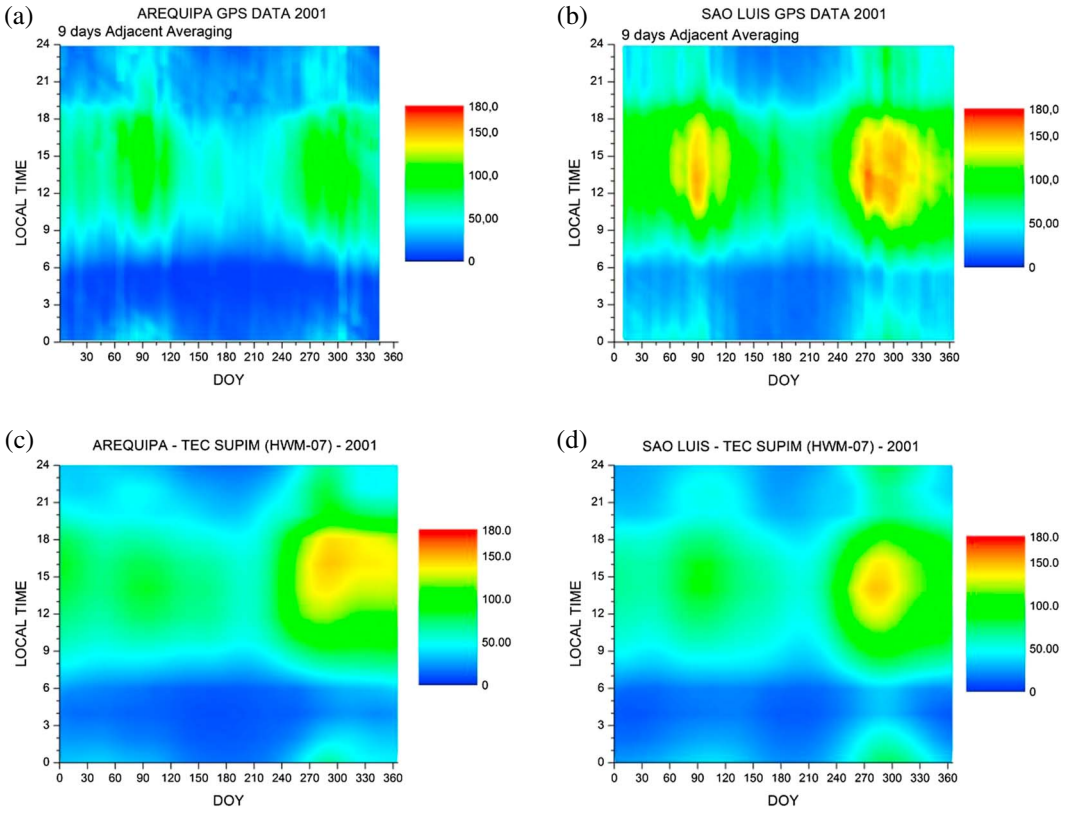

Figure 4. Local time versus day of the year (DOY) variation in the TEC over (a and c) Arequipa and over (b and d) São Luís during 2001. The seasonal variation may be noted. Figures 4a and 4b are the observational data of the GNSS TEC and Figures 4c and 4d are the corresponding results from the SUPIM.

Although the solar zenith angles during the March and the September equinoxes are the same, the ionosphere is known to present some differences between the two equinoxes under equivalent solar activity conditions which is known as the ionospheric equinoctial asymmetry [e.g., *Chen et al*., 2012; *Bailey et al*., 2000; *Balan et al*., 1998; *Kawamura et al*., 2002]. Such asymmetry may be originating from the equinoctial differences in neutral winds, thermospheric composition and density, and the electric fields, all of which control the electron density distribution. At least a part of the equinoctial asymmetry, in our 2001 TEC data, appears to be caused by the difference in the EUV ionization flux between the spring and autumn equinoxes, as may be verified from the fact that the 3 month averaged values of the F10.7 index were 166.3 and 216.0 (10^{-22} W m^{-2} Hz^{-1}) around 1 April and 1 October, respectively.

[19] Semiannual variation in the 10–17 LT daytime maximum of the TEC, similar to the results presented here, has been reported before for the Brazilian sector from geo stationary satellite radio beacon observations by VHF polarimeters by *Abdu et al*. [1996]. Such features in the TEC have also been discussed by other researchers, for example, *Liu et al*. [2009], *Batista and Abdu* [2004], *Lee et al*. [2010], and *Ma et al*. [2003], and therefore, they will not be discussed here further.

[20] As an important point, we may note in Figure 4 that the TEC values over São Luís are significantly larger than those over Arequipa, the values during September/October period being ~170 total electron content units (TECUs), 1 TECU = 10^{16} el m^{-2}, over São Luís and ~100 TECU over Arequipa, a difference of 70 TEC units. It is interesting to note that such difference in the TEC between São Luís and Arequipa is likely associated with the minima and maxima of the longitudinal four-peaked structure that we could observe in the topside Ni values shown in Figures 1 and 2. It should be noted, however, that the longitudinal variation in the topside Ni shown in Figure 2 is characterized by larger values over the west coast as compared to that over the east coast of South America while the TEC shows an opposite behavior. The reason for such opposite trends will be discussed in section 3.2. We may also note that this longitudinal difference in the TEC prevails for the whole day and the whole year, independent of the local time sector, season, or solar activity. However, it may be noted that the highest discrepancies between the TEC in São Luís and Arequipa occurs between 0900 LT and 1800 LT, and it is stronger close to the equinox; the largest discrepancy occurs during high solar activity as will be discussed later (see Figure 6), which could indicate that the nonmigrating tides might be more effective to modulate the *E* region dynamo during high solar activity. A clear demonstration of the longitudinal variation in the daytime TEC represented by its values at 15 LT during the months of September, October, and November of 2010 is shown in Figure 5; the solar flux for this period was nearly constant.

[21] Figure 6 shows the variation in the daytime TEC (12 LT values) as a function of the solar flux index F10.7 for the equinoctial months (every day from 15 February up to 15 May and from 15 August up to 15 November was

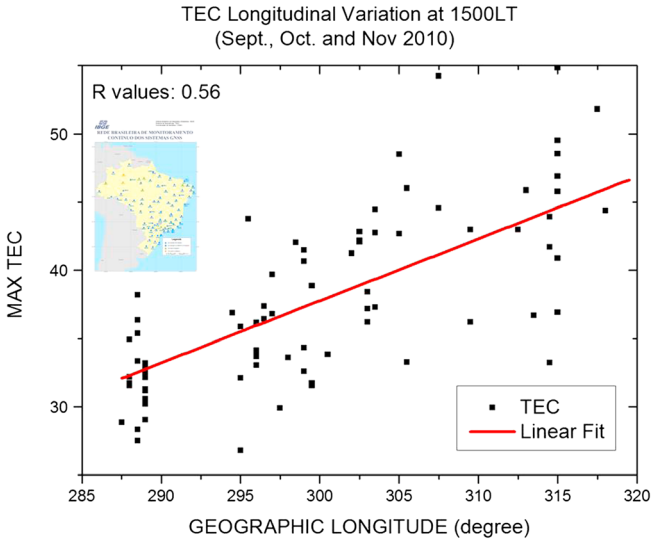

Figure 5. Longitudinal variation of the diurnal maximum of the TEC over Brazil.

considered). It may be observed in Figure 6 that for low solar flux values the TEC in São Luís is only slightly higher than that over Arequipa. However, with the increase in F10.7 the TEC over São Luís increases more rapidly than over Arequipa. This behavior may be quantified by noting that the TEC ratio between São Luís and Arequipa, (TEC_{SL}/TEC_{AREQ}) which is 1.3 during low solar activity, increased to 1.6 during high solar activity. Another way of quantifying that TEC over São Luís increase faster than over Arequipa in function of solar flux is by considering the slope coefficient for the linear fits of these data plots, its value being 0.63 for Sao Luis and 0.39 for AREQ. Obviously, the larger slope coefficient over São Luís leads to the significantly larger TEC over São Luís than over Arequipa during solar maximum years. This would suggest that the four-peaked structure pattern in the TEC is more dominant during the solar maximum years than during solar minimum years.

[22] It may be noted further that the TEC increase tends to saturate for very high solar flux values [see also *Batista et al.*, 1994; *Liu et al.*, 2009]. The same conclusion can also be drawn from the whole year data and from 1 year adjacent averaging with the whole year data (to eliminate the seasonal variation), although only the analyses of the equinox data were shown here.

[23] In order to explain what is causing the difference in the TEC intensity between São Luís and Arequipa, we used the SUPIM to model the low-latitude TEC distribution. Figures 4c and 4d show the model results of the TEC distribution plotted for each day of the year 2001 as a function of local time for São Luís in Figure 4d and for Arequipa in Figure 4c. These plots can now be compared with the corresponding observed TEC distribution plotted in Figures 4a and 4b that were discussed earlier.

[24] The results from SUPIM shown in Figures 4c and 4d were obtained using, as input to the model, the zonal electric field from *Scherliess and Fejer* [1999] empirical model and the horizontal thermospheric neutral wind as per the HWM-07 empirical model. Both the empirical models used as input do not contain in them any meaningful longitudinal variations due to nonmigrating tides. From the comparison between observational data and model results it can be seen that the SUPIM is able to reproduce well the TEC semiannual variation, characterized by the lowest TEC values during the southern winter and the highest TEC values during the equinoctial months. The SUPIM results also bring out well the equinoctial asymmetry in the TEC and the local time variation pattern characterized by the lowest values near the sunrise and highest values close to 1500 LT. However, in terms of the absolute TEC values these SUPIM runs are unable to reproduce the observed TEC values. The modeling results underestimate the TEC over São Luís and overestimate it over Arequipa. Thus, we note that the standard control parameters input to the SUPIM cannot simulate well the longitudinal difference in the TEC observed in the American longitude sector nor do the modeled TEC values agree with the observed values in absolute terms at the two locations.

[25] We will examine below the possible input factors used in the SUPIM runs that need to be modified in order to obtain agreement between the model and observational results. The ion production rate with related photochemistry is a fundamental input to the model. Additionally, the most important dynamic parameters input to the SUPIM that control the electron density distribution in the entire low-latitude ionosphere, and therefore the TEC, are the zonal electric field driving the plasma fountain (the vertical drift) and the thermospheric winds [*Abdu et al.*, 1990; *Balan and Bailey*, 1995; *Rishbeth*, 2000; *Abdu*, 2001; *Souza et al.*, 2000b; *Lin et al.*, 2005]. Thus, we will seek an explanation in terms of the zonal electric field and thermospheric winds for the longitudinal variation in the TEC and in the topside Ni observed in the American longitude sector. As regards the zonal electric field it is now well known that the nonmigrating tides that propagate to the mesosphere lower thermosphere heights modulate the *E* region dynamo electric field contributing to the four -peaked structure in the zonal electric field/vertical drift, the equatorial electrojet, and the *F* region plasma density distribution [*England*, 2012].

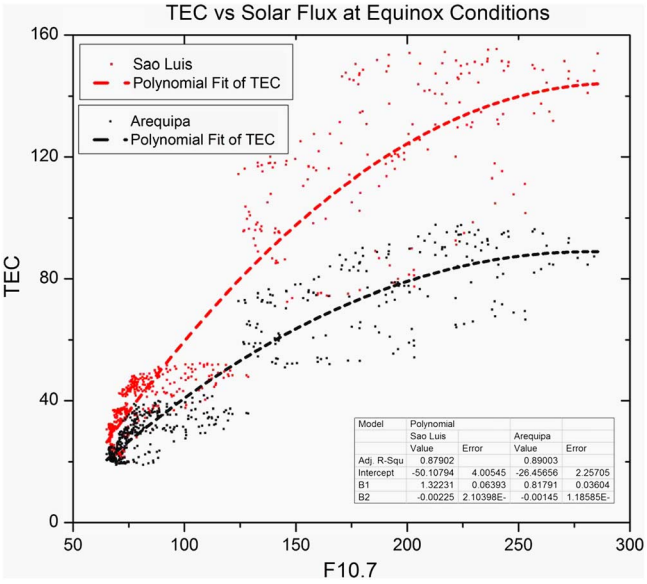

Figure 6. Solar flux effects on the TEC at noon (12 LT) over São Luís (red) and Arequipa (black) during equinoctial conditions.

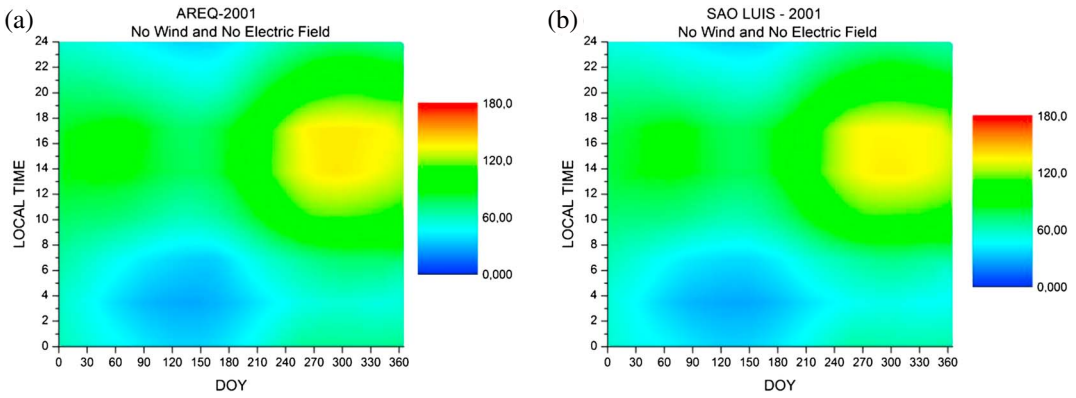

Figure 7. TEC seasonal versus local time variation over (a) Arequipa and over (b) São Luís obtained from the SUPIM runs that did not include the electric field and thermospheric wind but considered only the photochemistry (the ion production and loss effects).

[26] As a first step toward identifying the possible sources that could contribute to the longitudinal variation, we ran the SUPIM model for São Luís and Arequipa by neglecting the plasma transport process, that is, by putting zero terms for the zonal electric field and the thermospheric winds. In this way it is possible to evaluate any possible difference in the model output of electron density that may arise from the different degrees of photoionization at the two locations that are close to the magnetic equator but each separated by a few degrees away from the geographic equator. The results of these calculations are presented in Figures 7a and 7b for Arequipa and São Luís, respectively.

[27] As can be seen in Figure 7 the TEC distribution arising only from ion production and loss processes is almost the same over both stations. Therefore, we may conclude that any possible difference in the ion production rate due to the EUV radiation between the two locations and the associated photochemistry are not the cause of the observed longitudinal variation in the TEC. Consequently, the observed TEC differences between the two stations may be attributed to plasma transport effects.

3.1. Electric Field Effect

[28] The longitudinal variation in the vertical drift as suggested by *Hartman and Heelis* [2007] and *Kil et al.* [2009] is not appropriately represented in the Scherliess and Fejer empirical model of the vertical drift that we used as input to the SUPIM runs, whose results were presented in

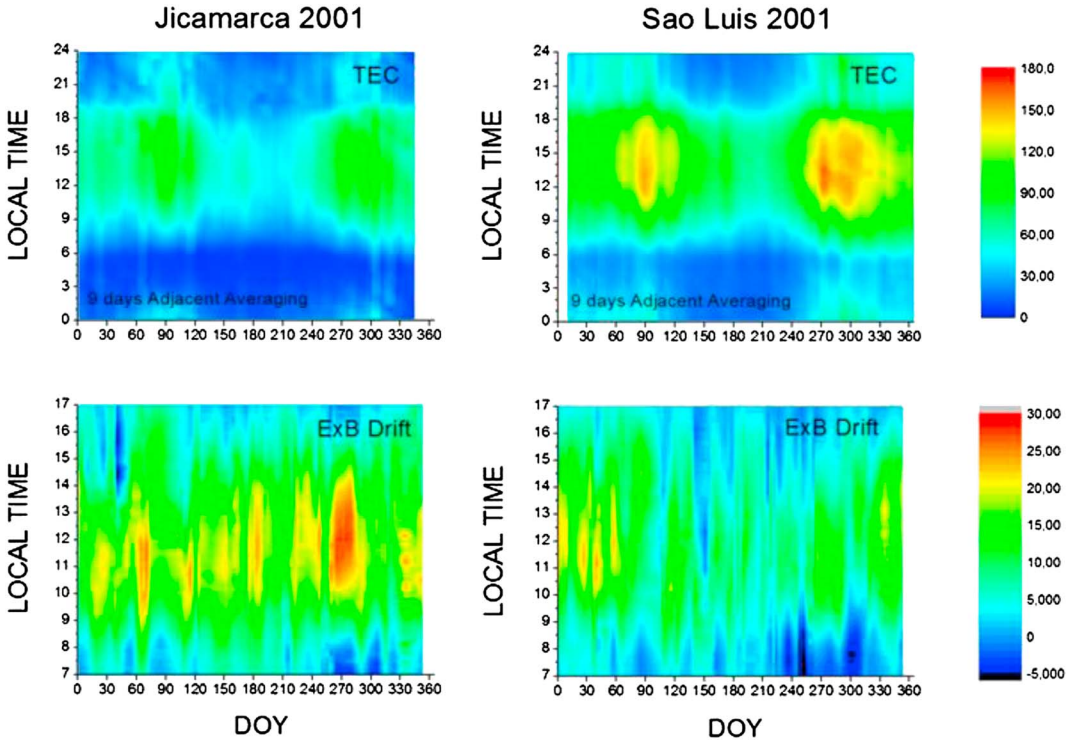

Figure 8. The TEC seasonal variation as a function of local time over (top, right) São Luís and (top, left) Arequipa; the corresponding seasonal versus local time variation in the vertical **E** × **B** drift velocities over (bottom, right) São Luís and (bottom, left) Jicamarca.

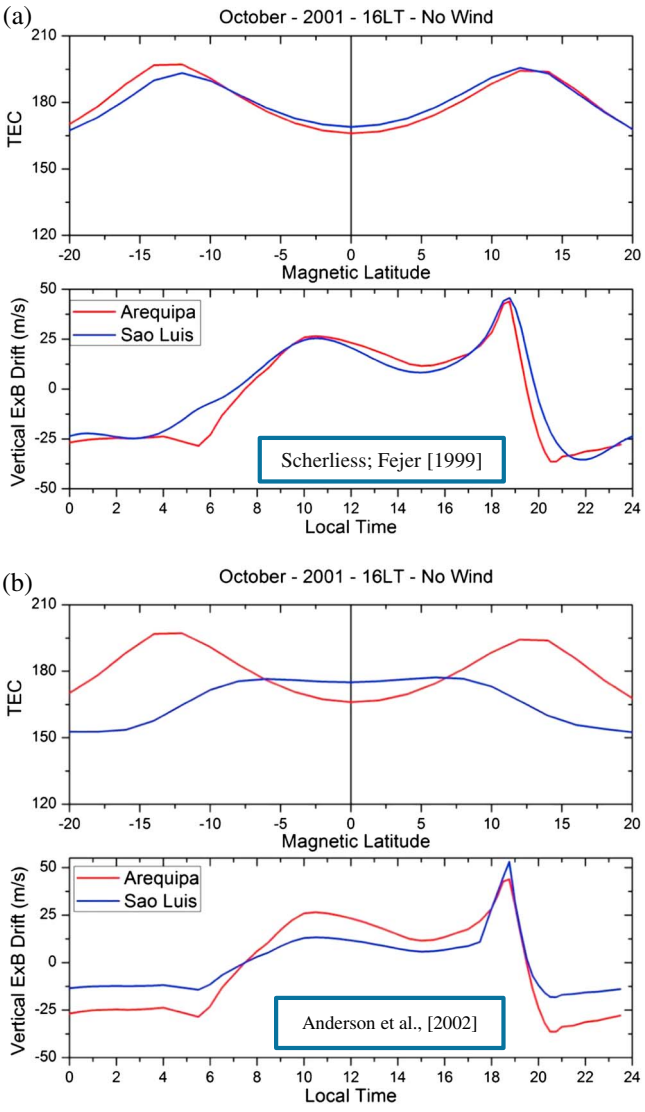

Figure 9. (a) TEC latitudinal variation estimated from SUPIM for the longitudes of São Luís (blue line) and Arequipa (red line) (top); corresponding $\mathbf{E} \times \mathbf{B}$ drift velocities used as an input in SUPIM (bottom). (b) Same results as in Figure 9a, except that the $\mathbf{E} \times \mathbf{B}$ drift velocity obtained from magnetometer (for the daytime) and ionosonde (for the evening) was used. The thermospheric wind was switched off for both Figures 9a and 9b.

Figures 4c and 4d. In order to have realistic $\mathbf{E} \times \mathbf{B}$ drift as input to the SUPIM we used ground-based magnetometer data from dip equatorial and off-equatorial sites in the longitudes of Arequipa and São Luís and calculated the daytime $\mathbf{E} \times \mathbf{B}$ drifts as was explained in section 2.3.

[29] The results are presented in Figure 8, which shows in the two top panels the local time variation of the observational TEC for each day of the year 2001 over São Luís (Figure 8 (top, right)) and Jicamarca representing Arequipa (Figure 8 (top, left)) (the same plots as in Figure 4). The $\mathbf{E} \times \mathbf{B}$ drift (to modify the input to the SUPIM) as obtained from the difference in the horizontal magnetic field component (ΔH) recorded at a dip equatorial station, and that over an off-equatorial station, is shown in Figure 8 (bottom, left) for Jicamarca, and in Figure 8 (bottom, right) for Sao Luis. Sixty-three days of data were linearly interpolated to form a full year of data for Jicamarca, whereas this procedure was not necessary for São Luís for which the date was available on most days of the year.

[30] We may note in Figure 8 that the $\mathbf{E} \times \mathbf{B}$ drift velocity over Jicamarca is generally larger than over São Luís, often by approximately a factor of 2, for example, during the period of September–October. Such behavior is in agreement with the $\mathbf{E} \times \mathbf{B}$ drift longitudinal variation due to the nonmigrating tides modulating the *E* region wind dynamo [*England*, 2012].

[31] We note in Figure 8 that while the TEC over São Luís is larger than the TEC over Arequipa, the vertical $\mathbf{E} \times \mathbf{B}$ drift velocity over São Luís is smaller than that over Arequipa/Jicamarca. This result may be explained as follows: The $\mathbf{E} \times \mathbf{B}$ plasma drift raises the ionization to higher altitudes over the equatorial region. Under the action of pressure gradient and gravity forces the uplifted plasma flows downward along the magnetic field lines to higher latitudes, where the enhanced plasma concentrations are responsible for the two ionization crests at ±15° latitude constituting the equatorial ionization anomaly (EIA). Right over the dip equator there is a reduced plasma concentration representing the ionization trough of the EIA. The depth of the ionization trough (that is, the reduction of the equatorial electron density and the TEC) should increase with increase in the vertical plasma drift. Thus, the higher $\mathbf{E} \times \mathbf{B}$ vertical drift causes the reduced TEC over Jicamarca compared to the smaller vertical drift that causes the larger TEC over São Luís.

[32] Based on the longitudinal variation of the TEC in the EIA trough region as described above, a corresponding longitudinal variation in the EIA crest is expected to be characterized by an opposite trend, that is, the crest intensity over west coast of South America should be stronger than over east coast of South America. Additionally, as mentioned in *Lin* et al., [2007], a stronger equatorward neutral wind helps to sustain the plasma at higher altitudes, resulting in an enhanced EIA strength. It is also noted that the equatorward neutral wind may result in equatorward movement of EIA crests. To address these questions we used the SUPIM also to calculate the TEC latitudinal distribution over São Luís and Arequipa.

[33] First, we performed a SUPIM simulation, modifying its $\mathbf{E} \times \mathbf{B}$ drift input as explained above, in order to understand if the observed longitudinal variation in the zonal electric field could be enough to explain the observed longitudinal difference in the TEC. The TEC latitudinal distribution in Figure 9a was obtained using the *Scherliess and Fejer* [1999] empirical zonal electric field model as an input to the SUPIM. The latitudinal distribution in Figure 9b was obtained using the vertical $\mathbf{E} \times \mathbf{B}$ drift calculated from magnetometer (daytime) and ionosonde (evening) data and complemented by Scherliess and Fejer model for night-morning period as was explained in section 2.3. The thermospheric wind was switched off in these simulations. Figures 9a (top) and 9b (top) show the TEC predicted by the SUPIM using the corresponding vertical drift (zonal electric field) model shown in the bottom. The blue line represents São Luís, and the red line represents Arequipa. In Figure 9a we may note that the use of the Scherliess and Fejer electric field model as an input to the SUPIM does not produce any significant longitudinal variation in the

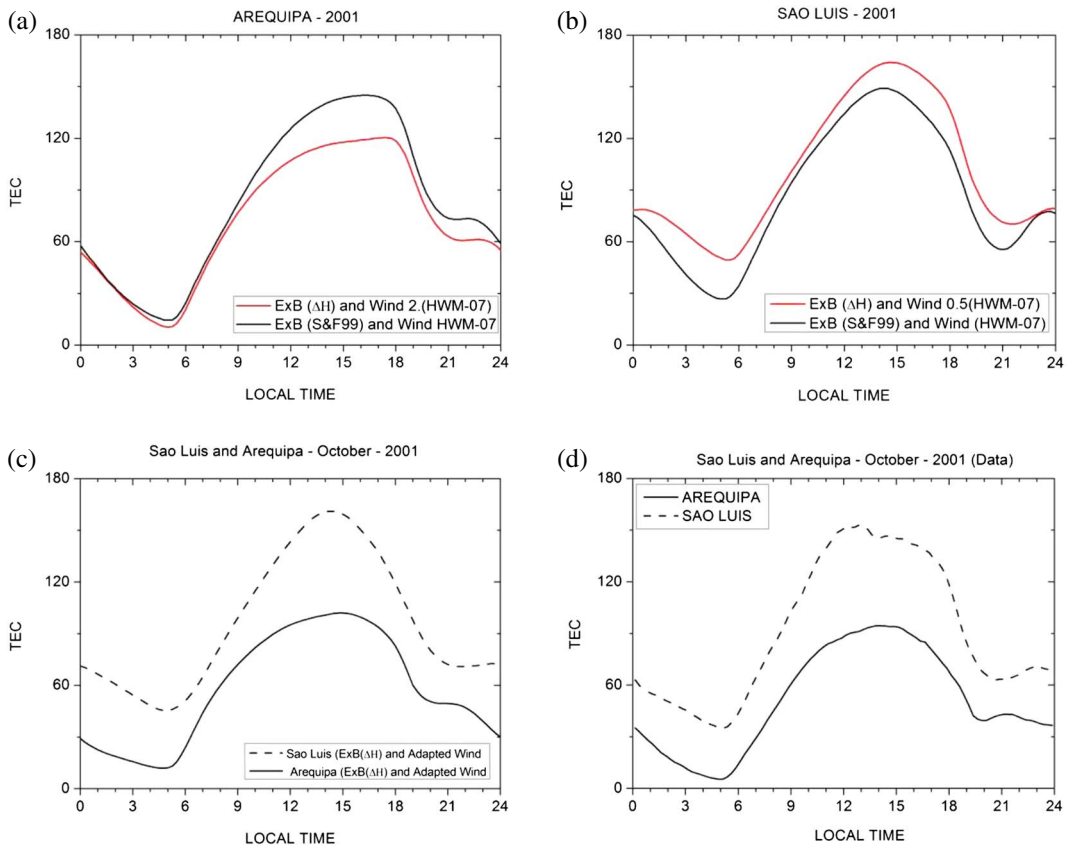

Figure 10. Local time variation of the TEC calculated from the SUPIM for different vertical drift and wind models: (a) the TEC over Arequipa obtained for (i) S-F vertical drift and the HWM07 wind models (red curve) compared with that obtained for (ii) the magnetometer + ionosonde (M-I) vertical drift and doubled the HWM07 winds (black curve); (b) the corresponding results for São Luís; (c) a comparison of the TEC local time variation between São Luís and Arequipa obtained for the model (iii) vertical drift and winds; (d) the observed TEC local time variations for the two locations.

TEC. However, using the new $\mathbf{E} \times \mathbf{B}$ drift (electric field) shown in the bottom plot of Figure 9b as input to the SUPIM, the equatorial TEC over São Luís becomes larger than over Arequipa, i.e., with the same tendencies seen in the observational data. It is also to be noted that the EIA crest simulated by the SUPIM is stronger over the west coast of South America than over the east coast of South America as to be expected. However, the difference in the equatorial TEC predicted by the SUPIM is not able to fully explain the difference observed in the GNSS TEC data that is shown in Figures 4a and 4b. To understand what is causing the overall difference, the contribution from thermospheric neutral winds is investigated in the following section.

3.2. Thermospheric Neutral Wind Effects

[34] Thermospheric neutral winds exhibit substantial spatial and temporal variations over a wide range of scales during geomagnetically quiet as well as disturbed periods. Such variations can produce large changes in the ionospheric plasma density, composition, temperature, and electrodynamics. *Titheridge* [1995] has shown that there is a positive latitudinal gradient in the quiet time thermospheric meridional wind, which means that over a low-latitude station, such as Arequipa, the meridional wind should be larger than over a geographic equatorial station, such as São Luís [see also *Emmert et al.*, 2002]. Further, the difference in ion density distribution between the two longitudes (west and east coast of south America) could cause difference in the degrees of ion drag effect and hence in the values of meridional winds at the two longitudes. Besides, there are evidences of the extended upward propagations of the nonmigrating tides, acting as a direct coupling agent between the troposphere and the thermosphere, which could longitudinally modulate the upper thermospheric wind amplitude due to the direct penetration of the nonmigrating tide to the *F* region height [*Lühr et al.*, 2007; *Talaat and Lieberman*, 2010; *Hagan et al.*, 2009; *Pedatella et al.*, 2011]. Such differences are not adequately represented in the HWM-07 model, which we have used in our SUPIM simulation. Therefore, to represent, at least in a gross way, the latitudinal and longitudinal difference in the winds, we used as input to the SUPIM the HWM-07 wind whose magnitude was doubled for the Arequipa meridian while it was halved for São Luís meridian.

[35] Figure 10 shows the local time variation of the TEC calculated by the SUPIM for São Luís and Arequipa for different combinations of the inputs $\mathbf{E} \times \mathbf{B}$ vertical drift and HWM winds, and a comparison of them with observational data. Figure 10a shows a comparison for Arequipa of the TEC obtained from the SUPIM runs by using (i) the Scherliess and Fejer (S-F) vertical drift model and the HWM-07 winds (black line) with that obtained by using (ii)

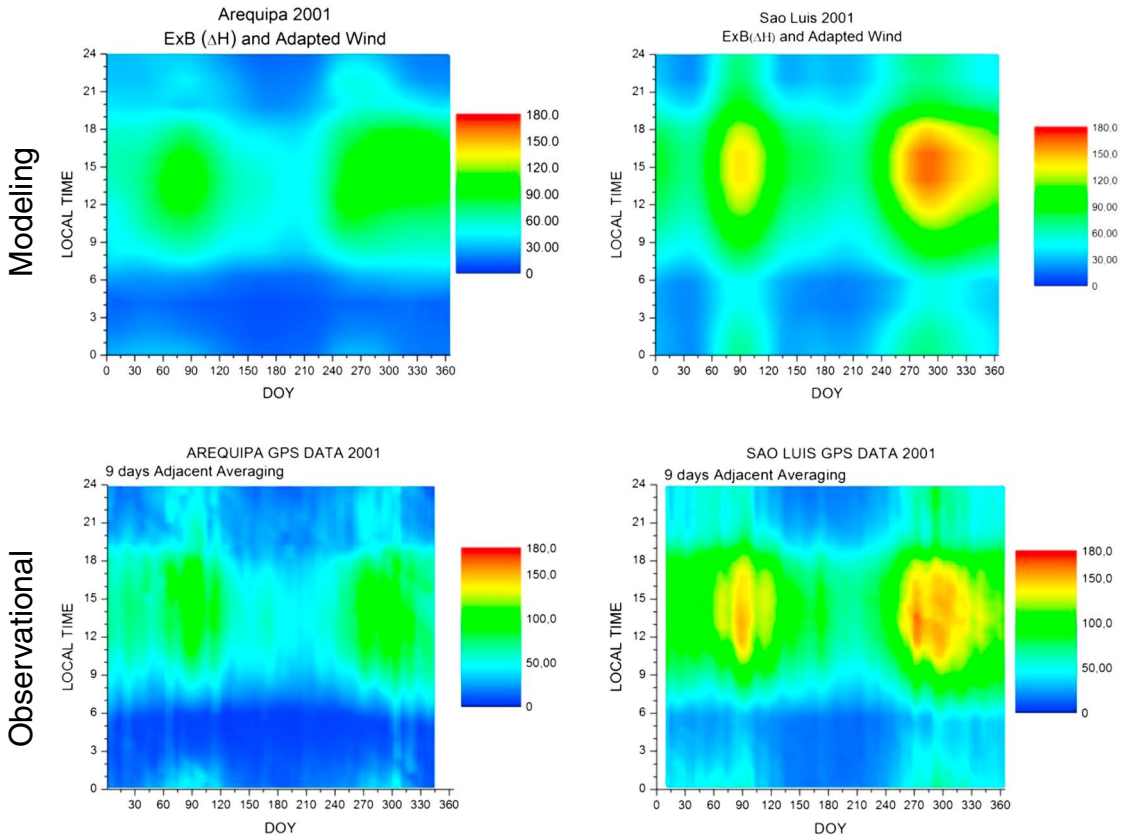

Figure 11. The SUPIM estimation for the TEC seasonal variation. (right) The TEC for São Luís and (left) for Arequipa may be observed. The **E** × **B** drift velocities used as an input in the SUPIM were obtained from magnetometer and ionosonde data, and an adapted thermospheric effective wind from the HWM-07 was also used.

the magnetometer plus the ionosonde (M-I) vertical drift and the doubled HWM-07 winds (red line). Figure 10b shows the corresponding results for São Luís, except for the halved HWM-07 winds that were used. We may note that while the SUPIM run with the model (ii) for vertical drift and winds results in generally enhanced TEC values (red curve) over São Luís, an opposite behavior (decreased TEC) is the result over Arequipa. In other words, by using a more realistic vertical drift and wind as input to the SUPIM the TEC values increased over São Luís while it decreased over Arequipa, approaching toward the observed trend in the TEC values over the two locations. Figure 10d shows the observational TEC; here solid line stands for Arequipa and dashed line for São Luís. An exception to the agreement can be noted near 19 LT (comparing Figures 10a and 10d), which appears to be caused by the inability of the model inputs to the SUPIM to simulate the TEC values over Arequipa in the evening hours. The vertical drift and/or the thermospheric winds used as input to the SUPIM appear to be inadequate at these hours over Arequipa.

[36] In order to quantitatively improve the simulation results for São Luís and Arequipa we used a model (iii) of vertical drift and wind input to the SUPIM. In model (iii) for Arequipa meridian we used the HWM-07 output multiplied by three as the effective wind for the whole day, except between 1500 and 2030 LT where we consider a constant effective wind as the triple of the HWM-07 at 1430 LT. We also changed the thermospheric wind over São Luís meridian, where from 0000 LT up to 0600 LT we used the HWM-07 multiplied by 0.2, between 0600 and 1400 LT the thermospheric wind was multiplied by 0.33, between 1400 and 2100 LT the HWM-07 output was not modified, and between 2100 and 2400 LT the wind was multiplied by 0.2. Figure 10c shows a comparison of the results of these SUPIM runs wherein we may note that the TEC values over São Luís (dashed curve) are, in general, higher than those over Arequipa (solid curve) at nearly all local times, which is very similar to the observed TEC variation over the two stations shown in Figure 10d.

[37] Overall, we may note from a comparison between Figures 10c and 10d that the SUPIM can now successfully predict the TEC longitudinal variation when more realistic values of the vertical drift and thermospheric winds are used as input to the model.

[38] It was noted that the longitudinal variation in the Ni observed by the DMSP F13 shown in Figure 1 presented larger values over the west coast as compared to that over the east coast of South America. The larger vertical drift over the Jicamarca appears to be responsible for the larger topside Ni values at the 840 km orbit of the DMSP satellite, although the TEC does not increase correspondingly. This situation may occur because of the lower densities near the F_2 peak resulting from the larger vertical drift. Over the east coast, on the other hand, the smaller vertical drift causes the smaller topside density at 840 km height maintaining larger Ni values near the F_2 peak, which contributed to the larger values of the observed TEC. Thus, our modified vertical drift appears to explain the longitudinal variation of the topside Ni as well.

[39] The TEC local time versus seasonal variation obtained from the SUPIM runs with the modified electric field and

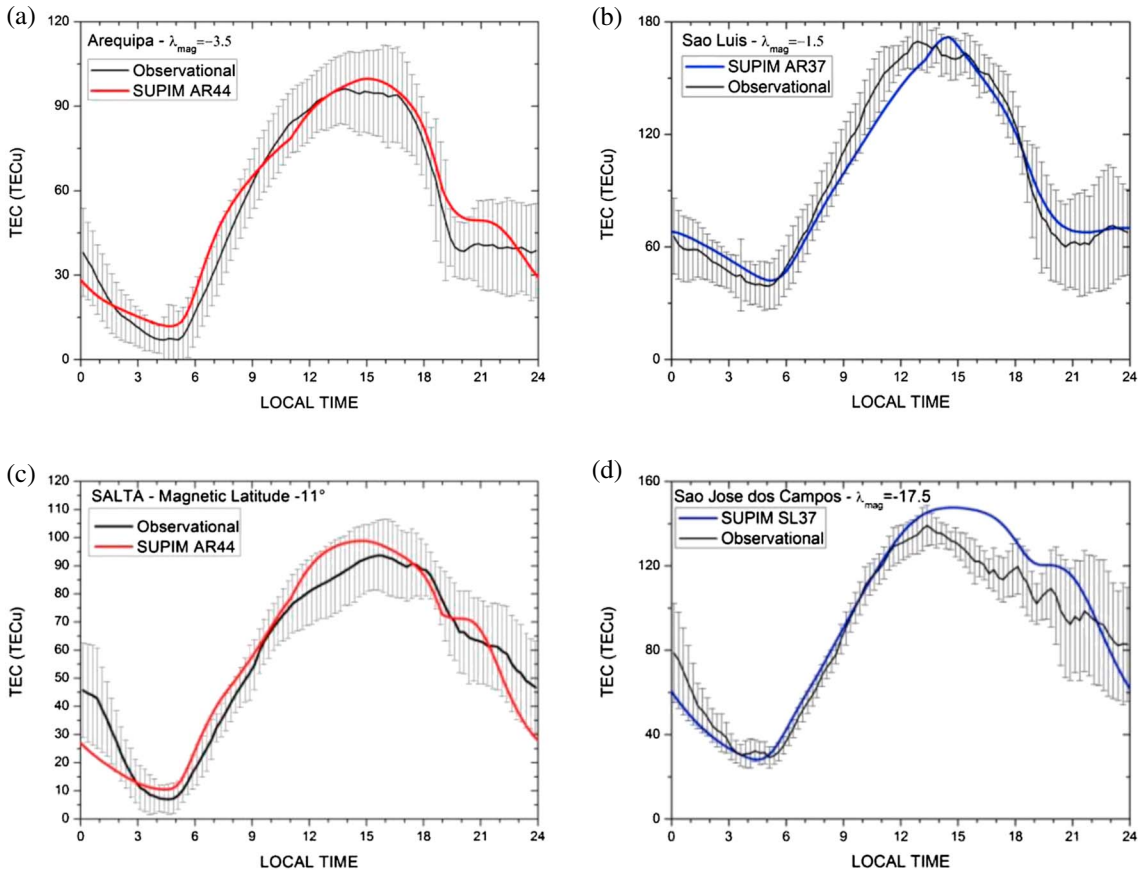

Figure 12. Comparison between observational and modeling results. (a) The comparison over Arequipa, (b) over São Luís, (c) over Salta, and (d) over São José dos Campos.

thermospheric neutral wind is shown in Figure 11 for the whole year in the same format as Figure 4. The SUPIM results shown in Figure 11 (top) can be compared with the observational data plotted in Figure 11 (bottom) (the same as that of Figure 4). It may be noted that the longitudinal variations in the TEC between São Luís and Arequipa is simulated by SUPIM when appropriate models of electric field and neutral winds are used, thereby strengthening the *Sagawa et al.* [2005] suggestion of the *E* region dynamo modulation by the nonmigrating tides as well as possibly the direct penetration of the nonmigrating tidal modes to thermospheric heights where the winds are also modified. The SUPIM simulated values are now in accordance with the observational data presented in Figure 4, which thus demonstrate that the TEC over São Luís is much larger than that over Arequipa during the whole year.

3.3. Thermospheric Wind Indirect Validation

[40] Using Figure 10 we have discussed the thermospheric wind modification (model (iii)) based on the HWM-07 code; however, such modifications require validation. Unfortunately, we have no daytime wind data available for the period of this study to validate such methodology. The limitations of the HWM-07 especially for the Southern Hemisphere are well known [see *Larsen and Fesen*, 2009; *Abdu et al.*, 2010]. However, the validation of the thermospheric winds over South America may be done using an indirect approach, similar to the methodology described by *de Souza* [1997] and *Souza et al.* [2000a]. It is recognized that the thermospheric winds are important for the latitudinal distribution of the ionospheric plasma. The validation of such winds, however, cannot be done by comparing the TEC calculated by the SUPIM with the observational data for a magnetic equator stations only (Figures 11 and 10c). There is a need to consider the latitudinal dependence of the TEC by comparing the data recorded simultaneously at magnetic equatorial and low-latitude stations with the corresponding TEC obtained from the SUPIM simulations.

[41] In an attempt to validate the TEC latitudinal distribution obtained from the SUPIM vis-a-vis the thermospheric wind, two low-latitude ground stations were selected, one situated on the east coast and the other on the west coast of South America. These stations are, respectively, São José dos Campos (−23.17°; 314.11°; *dip angle*: −32° (2001)) and Salta (−24.78°; 294.6°; dip angle: −24° (2001)).

[42] Figures 12a and 12c show, respectively, the TEC daily variation for the west coast of South America, being represented by Arequipa (close to the magnetic equator) and Salta (close to the EIA southern crest) for October 2001, where the black line is representing the observational monthly average values and its standard deviation bars and the red line shows the SUPIM modeling results. Figures 12b and 12d are similar to Figures 12a and 12c but representing the east coast of South America, being São Luís (magnetic equator) and São José dos Campos (EIA south crest) the chosen pair of station.

[43] From Figure 12a we may observe that the SUPIM (red line) is able to predict well the TEC over the magnetic equator

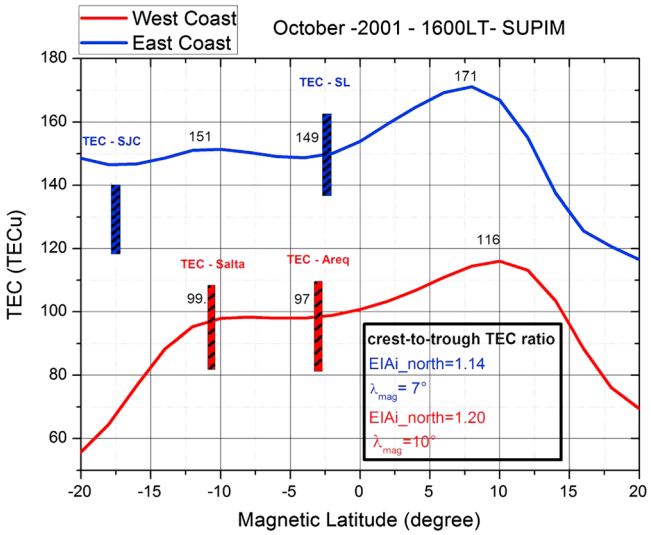

Figure 13. TEC latitudinal distribution over west coast (red line) and east coast (blue line) of South America.

(Arequipa), as well as we may note in Figure 12c that the SUPIM is representing adequately well the TEC behavior over Salta (low latitude). Since the zonal electric field methodology was already previously validated, we consider that the other dynamic parameter, i.e., thermospheric wind, is also validated from the good agreement reached between the observational and modeling result for both equatorial and low-latitude stations in the western longitudes of South America.

[44] Similarly, we can validate the transport effects (electric fields and neutral winds) on the east coast of South America. In Figure 12b we compare the SUPIM estimation (blue line) with the measured values of TEC (black line) over the equatorial sector, São Luís, and Figure 12d makes the same comparison for the southern crest of the EIA, that is, São José dos Campos. We note that the SUPIM is reasonably effective to estimate the TEC on the east coast of South America, as well, and thus indirectly validating our methodology to represent the neutral winds. We may point out, however, that the comparison between the observational data and model results over São José dos Campos (Figure 12d) shows a disagreement from 1400 to 1700 LT, which could be corrected by minor changes in the thermospheric wind.

[45] Since it appears that we have succeeded in developing an appropriate methodology to represent the effects of the plasma transport, the latitudinal distribution of the TEC on the east and west coast of South America was calculated with the SUPIM, using in this opportunity appropriate values for vertical drifts and thermospheric winds. Figure 13 illustrates the latitudinal distribution of the TEC for October 2001 at 1600 LT, with the blue profile representing the east coast (Brazilian meridian) and red line representing the west coast (Peruvian meridian). Vertical bars represent the standard deviation of the observed values at 1600 LT over São Luís (blue) and Arequipa (red) (equatorial stations), and the standard deviation of the observed values on the low-latitude stations in São José dos Campos (blue) and Salta (red).

[46] From Figure 13 we can observe the EIA development over South America, characterized by a trough at the magnetic dip equator flanked by two peaks, one on each side of the dip equator. We note that the EIA southern crest is significantly weakened over both the east and west coast. It seems that this is the first demonstration (based on observation and model simulation) showing that the TEC on the east coast is greater than on the west coast of South America over the entire latitudinal range, and not just around the magnetic equator. However, despite the TEC values being higher in the Brazilian sector, the intensity of the EIA (defined as average crest-to-trough ratio) appears to be a little higher on the west coast of South America. This can be seen also by the relatively larger latitudinal separation of the EIA crests on the west coast (see, for example, that the EIA north crest of the west coast is located at ~ 10° magnetic latitude, while the EIA north crest on the east coast is located at ~ 7° of magnetic latitude). A coherent response to the combination of different vertical drift and winds between the two sectors was thus obtained.

4. Summary and Conclusion

[47] The low-latitude ionosphere is a highly dynamic environment that exhibits significant variations with local time, altitude, latitude, longitude, season, solar activity, geomagnetic storms, and so on. In this paper our focus is on the longitudinal difference in the equatorial TEC values (that is, the TEC at the EIA trough) and the topside ion density values as observed between the west and east coast of South America. Our simulation by the SUPIM showed that the observed longitudinal trend cannot be explained when the existing standard model of the vertical drift (S-F model) and the horizontal winds (HWM-07) are used as input control parameters to the SUPIM. The presence of a four-peaked structure in the longitudinal variation of the ion density is now well established [*Sagawa et al*., 2005], as being caused by upward propagating nonmigrating tides and their modulation of the daytime *E* region dynamo, and as a consequence, the *F* region zonal electric field. The equinoctial epoch of our study is known to be better conditioned for the upward propagating nonmigrating DE3 tidal mode and therefore for the formation of well-defined longitudinal WN4 structure (see, for example, *Pedatella et al*. [2011]). It is not clear how the horizontal winds are modulated; however, the longitudinal differences in the ion drag added to the presence of the nonmigrating tides in the upper thermospheric wind must have an important component in the horizontal wind modulations. Such modulation effects appear to be not adequately accounted for the existing standard models of the vertical drift and thermospheric wind used as input to the SUPIM runs that failed to simulate the observed longitudinal trend in the TEC. We have attempted, with reasonable success, to account for these effects by appropriately modifying the vertical drift and horizontal winds as explained above, and such modified parameters, when input to the SUPIM, are shown to be capable of explaining the observational results on the longitudinal trends in the TEC and the topside Ni values.

[48] The main conclusions of this study may be summarized as follows:

[49] 1. The TEC variations near the dip equator, that is, at the equatorial ionization anomaly trough locations, in the American sector presents semiannual maxima, with the two peaks occurring during the equinoctial months. The semiannual maxima are stronger during the day hours than during the night hours.

[50] 2. The longitudinal variation in the TEC appears to be stronger during September/October equinox, which favors

the association of such feature to the WN4 structure arising from the upward propagating nonmigrating DE3 tidal mode.

[51] 3. A strong longitudinal variation in the daytime $\mathbf{E} \times \mathbf{B}$ vertical drift is present over the South American longitude sector, the vertical drift over the western sector, represented by Jicamarca, being stronger than that over the eastern sector, represented by São Luís, by approximately a factor of 2 during September/October 2001 period analyzed in this study.

[52] 4. A strong longitudinal variation is observed in the TEC and topside Ni. The SUPIM has not been able to simulate the longitude segment of the four-peaked structure in the TEC and Ni (in the American sector) when the zonal electric field model of *Scherliess and Fejer* [1999] is used as one of its driving input. The $\mathbf{E} \times \mathbf{B}$ velocity deduced from the magnetometer data, which should contain the nonmigrating tide effects, is found to be necessary for approaching to a better explanation of the observed longitudinal variation in the TEC.

[53] 5. Besides the longitudinal variation in the $\mathbf{E} \times \mathbf{B}$ drift, we have also proposed a strong longitudinal variation on the thermospheric wind, which may arise from the differences in the ion drag as well as due to the direct penetration of the nonmigrating tides to the *F* region heights. A test of the effect of the thermospheric neutral wind using SUPIM runs showed that a more intense wind causes decrease of the equatorial TEC enhancing the TEC at the EIA crest, while a decreased wind causes an opposite effect, that is, enhanced equatorial TEC and weakened EIA crest.

[54] 6. With the use of the vertical drift from magnetometer data that include the nonmigrating tidal effects and the thermospheric horizontal winds appropriately modified to account for its longitude-latitude dependence, the SUPIM is able to reproduce the longitudinal dependence of the TEC and topside Ni that closely resemble their observed features in the American longitude sector.

[55] 7. The longitudinal dependence of the low-latitude ionospheric density seems to show solar cycle dependence, presenting higher longitudinal variation during high solar activity.

[56] 8. While the TEC longitude variation arising from the four-peaked structures in the equatorial ionosphere is more active during daytime due to the *E* region dynamo modulation, its presence during nighttime evident in our data appears to be occurring due to the sustenance of the *F* layer in a higher height, where the recombination rate is smaller.

[57] 9. The TEC over the whole latitudinal distribution of east coast of South America is larger than over the west coast of South America. This behavior was observed in both observational and modeling results, which must be caused due to the longitudinal difference in the thermospheric meridional wind in combination to the longitudinal difference of the plasma vertical drift over South America.

[58] **Acknowledgments.** P.A.B Nogueira acknowledges the support from Conselho Nacional de Desenvolvimento Científico e Tecnológico (CNPQ) for his Ph.D. program through process 141.526/2010-6. This work has also been supported by the Fundação de Amparo a Pesquisa do Estado de São Paulo (2013/01924-1). C.M. Denardini thanks CNPq/MCTI (grant 305242/2011-3) and FAPESP (grant 2012/08445-9). We would like to acknowledge the NOAA for the F10.7 data availability. We gratefully acknowledge the Center for Space Sciences at the University of Texas at Dallas and the U.S. Air Force for providing the DMSP thermal plasma data. The Jicamarca Radio Observatory is a facility of the Instituto Geofisico del Peru operated with support from the NSF AGS-0905448 through Cornell University.

[59] Robert Lysak thanks the reviewers for their assistance in evaluating this paper.

References

Abdu, M. A. (2001), Outstanding problems in the equatorial ionosphere thermosphere electrodynamics relevant to spread F, *J. Atmos. Sol. Terr. Phys.*, *63*, 869–884.

Abdu, M. A., G. O. Walker, B. M. Reddy, J. H. A. Sobral, B. G. Fejer, T. Kikuchi, N. B. Trivedi, and E. P. Szuszczevicz (1990), Electric field versus neutral wind control of the equatorial anomaly under quiet and disturbed conditions: A global perspective, *Ann. Geophys.*, *8*(6), 419–430.

Abdu, M. A., I. S. Batista, and J. R. de Souza (1996), An overview of IRI-observational data comparison in American (Brazilian) low latitude ionosphere, *Adv. Space Res.*, *18*(6), 13–22.

Abdu, M. A., I. S. Batista, A. J. Carrasco, and C. G. M. Brum (2005), South Atlantic magnetic anomaly ionization: A review and a new focus on electrodynamic effects in the equatorial ionosphere, *J. Atmos. Sol. Terr. Phys.*, *67*, 1643–1657.

Abdu, M. A., I. S. Batista, C. G. M. Brum, J. W. MacDougall, A. M. Santos, J. R. de Souza, and J. H. A. Sobral (2010), Solar flux effects on the equatorial evening vertical drift and meridional winds over Brazil: A comparison between observational data and the IRI model and the HWM representations, *Adv. Space Res.*, *46*, 1078–1085.

Anderson, D., A. Anghel, K. Yumoto, M. Ishitsuka, and E. Kudeki (2002), Estimating daytime vertical $\mathbf{E} \times \mathbf{B}$ drift velocities in the equatorial F-region using ground-based magnetometer observations, *Geophys. Res. Lett.*, *29*(12), 1596, doi:10.1029/2001GL014562.

Anderson, D., A. Anghel, J. Chau, K. Yumoto, A. Bhattacharyya, and S. Alex (2006), Daytime, low latitude, vertical $\mathbf{E} \times \mathbf{B}$ drift velocities, inferred from ground-based magnetometer observations in the Peruvian, Philippine and Indian longitude sectors under quiet and disturbed conditions, in *The Solar Influence on the Heliosphere and Earth's Environment: Recent Progress and Prospects*, edited by N. Gopalswamy and A. Bhattacharyya, pp. 389–394, Quest Publications, Goa, India.

Bailey, G. J., and N. Balan (1996), Some modelling studies of the equatorial ionosphere using the Sheffield University Plasmasphere Ionosphere Model, *Adv. Space Res.*, *18*(6), 59–68.

Bailey, G. J., and R. Sellek (1990), A mathematical model of the Earth's plasmasphere and its application in a study of He + at L = 3, *Ann. Geophys.*, *8*(3), 171–189.

Bailey, G. J., R. J. Moffett, and J. A. Murphy (1978), Interhemispheric flow of thermal plasma in a closed magnetic flux tube at mid-latitudes under sunspot minimum conditions, *Planet. Space Sci.*, *26*, 753–765.

Bailey, G. J., R. Sellek, and Y. Rippeth (1993), A modeling study of the equatorial topside ionosphere, *Ann. Geophys.*, *11*(4), 263–272.

Bailey, G. J., N. Balan, and Y. Z. Su (1997), The Sheffield University ionosphere-plasmasphere model—A review, *J. Atmos. Sol. Terr. Phys.*, *59*(13), 1541–1552.

Bailey, G. J., Y. Z. Su, and K.-I. Oyama (2000), Yearly variations in the low-latitude topside ionosphere, *Ann. Geophys.*, *18*, 789–798, doi:10.1007/s00585-000-0789-0.

Balan, N., and G. J. Bailey (1995), Equatorial plasma fountain and its effects: Possibility of an additional layer, *J. Geophys. Res.*, *100*(A11), 21,421–21,432.

Balan, N., G. J. Bailey, K. S. V. Subbaro, M. A. Abdu, and P. B. Rao (1996), Model comparisons of equatorial plasma fountain and equatorial anomaly at three locations, *Adv. Space Res.*, *18*, 69–78.

Balan, N., Y. Otsuka, G. Bailey, and S. Fukao (1998), Equinoctial asymmetries in the ionosphere and thermosphere observed by the MU radar, *J. Geophys. Res.*, *103*, 9481–9495.

Bankov, L., R. Heelis, M. Parrot, J.-J. Berthelier, P. Marinov, and A. Vassileva (2009), WN4 effect on longitudinal distribution of different ion species in the topside ionosphere at low latitudes by means of DEMETER, DMSP-F13 and DMSP-F15 data, *Ann. Geophys.*, *27*, 1–10.

Batista, I. S., and M. A. Abdu (2004), Ionospheric variability at Brazilian low and equatorial latitudes: Comparison between observations and IRI model, *Adv. Space Res.*, *34*, 1894–1900.

Batista, I. S., J. R. Souza, M. A. Abdu, and E. R. de Paula (1994), Total electron-content at low latitudes and its comparison with the IRI90, *Adv. Space Res.*, *14*(12), 87–90, doi:10.1016/0273-1177(94)90246.

Bittencourt, J. A., and M. A. Abdu (1981), Theoretical comparison between apparent and real vertical ionization drift velocities in the equatorial F region, *J. Geophys. Res.*, *86*(A4), 2451–2454.

Chen Y., L. Liu, W. Wan, and Z. Ren (2012), Equinoctial asymmetry in solar activity variations of NmF2 and TEC, *Ann. Geophys.*, *30*, 613–622.

Denardini, C. M., H. C. Aveiro, P. D. S. C. Almeida, L. C. A. Resende, L. M. Guizelli, J. Moro, J. H. A. Sobral, and M. A. Abdu (2011), Daytime efficiency and characteristic time scale of interplanetary electric fields penetration to equatorial latitude ionosphere, *J. Atmos. Sol. Terr. Phys.*, *73*, 1555–1559.

de Souza, J. R. (1997), Modelagem ionosferica em baixas latitudes no Brasil tese (doutorado)- INPE, 1997 - São José dos Campos, SP: INPE, 154302432 (INPE-6395-TDI/611).

Dow, J. M., R. E. Neilan, and G. Gendt (2005), The international GPS service (IGS): Celebrating the 10th anniversary and looking to the next decade, *Adv. Space Res.*, *36*(3), 320–326, doi:10.1016/j.asr.2005.05.125.

Drob, D. P., et al. (2008), An empirical model of the Earth's horizontal wind fields: HWM07, *J. Geophys. Res.*, *113*, A12304, doi:10.1029/2008JA013668.

Emmert, J. T., Fejer, B. G., Shepherd, G. G., and Solheim, B. H. (2002), Altitude dependence of middle and low-latitude daytime thermospheric disturbance winds measured by WIND II, *J. Geophys. Res. 107*(A12), 1483, doi:10.1029/2002JA009646.

England, S. L. (2012), A review of the effects of non-migrating atmospheric tides on the Earth's low-latitude ionosphere, *Space Sci. Rev.*, *168*, 211–236, doi:10.1007/s11214-011-9842-4.

England, S. L., S. Maus, T. J. Immel, and S. B. Mende (2006), Longitudinal variation of the E-region electric fields caused by atmospheric tides, *Geophys. Res. Lett.*, *33*, L21105, doi:10.1029/2006GL027465.

Forbes, J. M., X. Zhang, S. Palo, J. Russell, C. J. Mertens, and M. Mlynczak (2008), Tidal variability in the ionospheric dynamo region, *J. Geophys. Res.*, *113*, A02310, doi:10.1029/2007JA012737.

Forbes, J. M., S. L. Bruinsma, X. Zhang, and J. Oberheide (2009), Surface-exosphere coupling due to thermal tides, *Geophys. Res. Lett.*, *36*, L15812, doi:10.1029/2009GL038748.

Hagan, M. E., Maute, A., Roble, R. G., Richmond, A. D., Immel, T. J., and England, S. L. (2007), Connections between deep tropical clouds and the Earth's ionosphere, *Geophys. Res. Lett.*, *34*, L20109, doi:10.1029/2007GL030142.

Hagan, M. E., A. Maute, and R. G. Roble (2009), Tropospheric tidal effects on the middle and upper atmosphere, *J. Geophys. Res.*, *114*, A01302, doi:10.1029/2008JA013637.

Hartman, W. A., and R. A. Heelis (2007), Longitudinal variations in the equatorial vertical drift in the topside ionosphere, *J. Geophys. Res.*, *112*, A03305, doi:10.1029/2006JA011773.

Häusler, K., H. Lühr, M. E. Hagan, A. Maute, and R. G. Roble (2010), Comparison of CHAMP and TIME-GCM nonmigrating tidal signals in the thermospheric zonal wind, *J. Geophys. Res.*, *115*, D00I08, doi:10.1029/2009JD012394.

Immel, T. J., E. Sagawa, S. L. England, S. B. Henderson, M. E. Hagan, S. B. Mende, H. U. Frey, C. M. Swenson, and L. J. Paxton (2006), Control of equatorial ionospheric morphology by atmospheric tides, *Geophys. Res. Lett.*, *33*, L15108, doi:10.1029/2006GL026161.

Kawamura, S., Balan, N., Otsuka, Y., and Fukao, S. (2002), Annual and semiannual variations of the midlatitude ionosphere under low solar activity, *J. Geophys. Res.*, *107*(A8), 1166, doi:10.1029/2001JA000267.

Kil, H., E. R. Talaat, S.-J. Oh, L. J. Paxton, S. L. England, and S.-J. Su (2008), Wave structures of the plasma density and $\mathbf{E} \times \mathbf{B}$ drift in low-latitude F region, *J. Geophys. Res.*, *113*, A09312, doi:10.1029/2008JA013106.

Kil, H., S.-J. Oh, L. J. Paxton, and T.-W. Fang (2009), High-resolution vertical $\mathbf{E} \times \mathbf{B}$ drift model derived from ROCSAT-1 data, *J. Geophys. Res.*, *114*, A10314, doi:10.1029/2009JA014324.

Larsen, M. F., and C. G. Fesen (2009), Accuracy issues of the existing thermospheric wind models: Can we rely on them in seeking solutions to wind-driven problems?, *Ann. Geophys.*, *27*, 2277–2284.

Lee, C. C., Y. J. Chuo, and F. D. Chu (2010), Climatology of total electron content near the dip equator under geomagnetic quiet-conditions, *J. Atmos. Sol. Terr. Phys.*, *72*, 207–212, doi:10.1016/j.jastp.2009.11.011.

Lin, C. H., A. D. Richmond, R. A. Heelis, G. J. Bailey, G. Lu, J. Y. Liu, H. C. Yeh, and S.-Y. Su (2005), Theoretical study of the low- and midlatitude ionospheric electron density enhancement during the October 2003 superstorm: Relative importance of the neutral wind and the electric field, *J. Geophys. Res.*, *110*, A12312, doi:10.1029/2005JA011304.

Lin, C. H., W. Wang, M. E. Hagan, C. C. Hsiao, T. J. Immel, M. L. Hsu, J. Y. Liu, L. J. Paxton, T. W. Fang, and C. H. Liu (2007), Plausible effect of atmospheric tides on the equatorial ionosphere observed by the FORMOSAT-3/COSMIC: Three-dimensional electron density structures, *Geophys. Res. Lett.*, *34*, L11112, doi:10.1029/2007GL029265.

Lin, C. H., W. Wang, M. E. Hagan, C. C. Hsiao, T. J. Immel, M. L. Hsu, J. Y. Liu, L. J. Paxton, T. W. Fang, and C. H. Liu (2007a), Plausible effect of atmospheric tides on the equatorial ionosphere observed by the FORMOSAT-3/COSMIC: Three dimensional electron density structures, *Geophys. Res. Lett.*, *34*, L11112, doi:10.1029/2007GL029265.

Lin, C. H., C. C. Hsiao, J. Y. Liu, and C. H. Liu (2007b), Longitudinal structure of the equatorial ionosphere: Time evolution of the four-peaked EIA structure, *J. Geophys. Res.*, *112*, A12305, doi:10.1029/2007JA012455.

Liu, H., and S. Watanabe (2008), Seasonal variation of the longitudinal structure of the equatorial ionosphere: Does it reflect tidal influences from below?, *J. Geophys. Res.*, *113*, A08315, doi:10.1029/2008JA013027.

Liu, L., Wan, W., Ning, B., and Zhang, M. L. (2009), Climatology of the mean total electron content derived from GPS global ionospheric maps, *J. Geophys. Res.*, *114*, A06308, doi:10.1029/2009JA014244.

Lühr, H., K. Häusler, and C. Stolle (2007), Longitudinal variation of F region electron density and thermospheric zonal wind caused by atmospheric tides, *Geophys. Res. Lett.*, *34*, L16102, doi:10.1029/2007GL030639.

Lühr, H., M. Rother, K. Häusler, P. Alken, and S. Maus (2008), The influence of nonmigrating tides on the longitudinal variation of the equatorial electrojet, *J. Geophys. Res.*, *113*, A08313, doi:10.1029/2008JA013064.

Ma, R., J. Xu, and H. Liao (2003), The features and a possible mechanism of semiannual variation in the peak electron density of the low latitude F2 Layer, *J. Atmos. Sol. Terr. Phys.*, *65*, 47–57.

Mannucci, A. J., B. D. Wilson, D. N. Yuan, C. H. Ho, U. J. Lindqwister, and T. F. Runge (1998), A global mapping technique for GPS-derived ionospheric total electron content measurements, *Radio Sci.*, *33*, 565–582.

Oberheide, J., J. M. Forbes, X. Zhang, and S. L. Bruinsma (2011), Wave-driven variability in the ionosphere-thermosphere-mesosphere system from TIMED observations: What contributes to the "wave 4"?, *J. Geophys. Res.*, *116*, A01306, doi:10.1029/2010JA015911.

Pancheva, D., and P. Mukhtarov (2010), Strong evidence for the tidal control on the longitudinal structure of the ionospheric F-region, *Geophys. Res. Lett.*, *37*, L14105, doi:10.1029/2010GL044039.

Pedatella, N. M., J. M. Forbes, A. Maute, A. D. Richmond, T.-W. Fang, K. M. Larson, and G. Millward (2011). Longitudinal variations in the F region ionosphere and the topside ionosphere-plasmasphere: Observations and model simulations, *J. Geophys. Res.*, *116*, A12309, doi:10.1029/2011JA016600.

Picone J. M., A. E. Hedin, D. P. Drob, and A. C. Aikin (2002), NRLMSISE-00 empirical model of the atmosphere: Statistical comparisons and scientific issues, *J. Geophys. Res.*, *107*(A12), 1468, doi:10.1029/2002JA009430.

Richards, P. G., J. A. Fennelly, and D. G. Torr (1994), EUVAC: A solar EUV flux model for aeronomic calculations, *J. Geophys. Res.*, *99*, 8981–8992.

Rishbeth, H. (2000), The equatorial F-layer: Progress and puzzles, *Ann. Geophys.*, *18*, 730–739.

Sagawa, E., T. J. Immel, H. U. Frey, and S. B. Mende (2005), Longitudinal structure of the equatorial anomaly in the nighttime ionosphere observed by IMAGE/FUV, *J. Geophys. Res.*, *110*, A11302, doi:10.1029/2004JA010848.

Scherliess, L., and B. G. Fejer (1999), Radar and satellite global equatorial F region vertical drift model, *J. Geophys. Res.*, *104*(A4), 6829–6842.

Scherliess, L., D. C. Thompson, and R. W. Schunk (2008), Longitudinal variability of low-latitude total electron content: Tidal influences, *J. Geophys. Res.*, *113*, A01311, doi:10.1029/2007JA012480.

Souza, J. R., M. A. Abdu, I. S. Batista, and G. J. Bailey (2000a), Determination of vertical plasma drift and meridional wind using the Sheffield University plasmasphere ionosphere model and ionospheric data at equatorial and low latitudes in Brazil: Summer solar minimum and maximum conditions, *J. Geophys. Res.*, *105*(A6), 12,813–12,821.

Souza, J. R., G. J. Bailey, M. A. Abdu, and I. S. Batista (2000b), Ionospheric modeling at low latitudes over Brazil during summer solar minimum, *Adv. Space Res.*, *25*, 133–138.

Talaat, E. R., and R. S. Lieberman (2010), Direct observations of nonmigrating diurnal tides in the equatorial thermosphere, *Geophys. Res. Lett.*, *37*, L04803, doi:10.1029/2009GL041845.

Titheridge, J. E. (1995), Winds in the ionosphere—A review, *J. Atmos. Sol. Terr. Phys.*, *57*(14), 1681–1714.

Wan, W., L. Liu, X. Pi, M. L. Zhang, B. Ning, J. Xiong, and F. Ding (2008), Wavenumber-4 patterns of the total electron content over the low latitude ionosphere, *Geophys. Res. Lett.*, *35*, L12104, doi:10.1029/2008GL033755.